Fast Segmentation of Focal Liver Lesions in Contrast-Enhanced Ultrasound Data

Spyridon Bakas[1]
S.Bakas@kingston.ac.uk
Katerina Chatzimichail[2]
Katerina@hcsl.com
Bastien Labbé[3]
Bast.Labbe@gmail.com
Gordon J. A. Hunter[1]
G.Hunter@kingston.ac.uk
Paul S. Sidhu[4]
Paulsidhu@nhs.net
Dimitrios Makris[1]
D.Makris@kingston.ac.uk

[1] Digital Imaging Research Centre
Faculty of Science, Engineering & Computing
Kingston University - London - U.K.

[2] Evgenidion Hospital
National & Kapodistrian University
Athens - Greece

[3] Acquisition & Image Processing
Télécom Physique Strasbourg
Strasbourg - France

[4] King's College Hospital
Denmark Hill - London - U.K.

Abstract

Assessment of focal liver lesions (FLLs) in Contrast-Enhanced Ultrasound data requires initialisation tasks that are currently performed manually by experienced radiologists. These tasks lead to subjective results, are time-consuming and prone to misinterpretation and human error. This paper describes an attempt to improve this clinical practice by proposing a complete pipeline for the automation of initialisation tasks, such as the identification of a frame where the FLL is well-distinguished, the segmentation of the FLL and the conical area including the ultrasonographic image. The currently proposed novel contribution to automate the FLL segmentation is a fast two-step method, initialised only by a single seed-point, which firstly approximates the FLL by an ellipse and then further refines its shape by iteratively classifying boundary pixels.

1 Introduction

Around 47,000 deaths occur annually in the EU due to primary liver cancer, the incidence rate of which is 6.2 and 2.4 per 100,000 people for males and for females, respectively [3]. Contrast-Enhanced Ultrasound (CEUS) is recognised as the most cost-efficient imaging solution for distinguishing between benign and malignant focal liver lesions (FLLs) [11], since it is easy to perform, and uses portable and relatively low cost equipment that allows its presence in every clinic and even at the bedside. Furthermore, CEUS has gained acceptance for the detection and characterisation of very small FLLs –i.e. at the very early/premature stages– with diagnostic accuracy exceeding 95% for the evaluation of malignancies [9].

Radiologists routinely detect, localise, monitor and evaluate FLLs in CEUS video recordings manually, through a very time-consuming series of tasks. These include the identification of a reference frame, where the FLL is sufficiently represented and well-distinguished

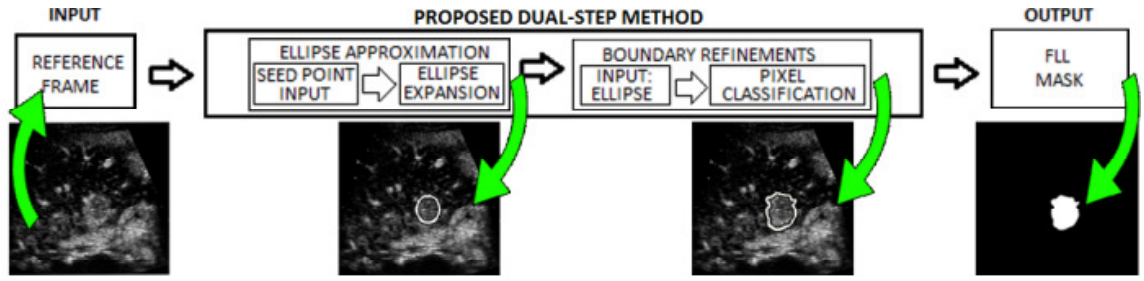

Figure 1: Pipeline of the proposed two-step method for the FLL segmentation.

from the remainder of the image plane in order to manually segment it, and eventually classify it as benign or malignant by monitoring the relative changes of brightness intensity of different regions of interest (ROIs) over time, i.e. their dynamic behaviour [12]. Each of these tasks requires a high level of expertise and provides operator-dependent results, which discourage radiologists from using the technique.

The tasks of monitoring and evaluating the dynamic behaviour of an FLL over the duration of a CEUS recording have been addressed by different solutions [1, 7, 10]. However, all of them assume the existence of prior initialised ROIs, such as the FLL and a larger area (i.e. US mask) including both the FLL and the surrounding healthy liver tissue (i.e. the parenchyma) in a reference frame. The selection of such a frame, as well as the automatic segmentation of the US mask have been addressed in [2] and [1], respectively. However, no solution has ever been suggested specifically for segmenting the FLL shape in a single frame of a CEUS recording. Thus, an expert is still needed to manually annotate the FLL in a frame, after following the standard care protocol. This manual procedure leads to subjective results, is time-consuming, and prone to misinterpretation and human error.

Therefore, automation of the process is highly desirable. Current approaches for segmentation of different tissues in medical images (e.g. snakes [4], level-sets [5]) are impractical due to either slow convergence through the need to optimise a large number of coefficients, or their dependence on a manual initialisation close to the actual boundaries [6]. This paper describes a complete pipeline to automate the initialisation tasks required for evaluating an FLL, whilst focusing on the FLL segmentation, in an attempt to improve the clinical practice by assisting the radiologists to make a diagnosis more easily and with greater confidence.

2 Methodology

The proposed pipeline first segments the US mask, by considering an intensity change detection as in [1] and then automatically identifies the optimal reference frame as in [2]. According to radiologists, this frame is expected to be the one with the maximum contrast between FLL and parenchyma.

A novel two-step method is then proposed to segment the FLL boundaries on the reference frame. Firstly, an enhanced version of a fast active ellipse model (AE) is used to approximate the FLL by an ellipse, initialised only by a single seed-point. Such an approximation is appropriate due to the FLL being roughly an ellipsoid by definition [11]. Thus, any 2D representation of an FLL results in an approximately elliptical shape. Secondly, the FLL segmentation is further refined automatically by iteratively classifying boundary pixels according to a probabilistic model of the FLL and the parenchyma intensities.

2.1 Ellipse Approximation

A Gaussian distribution model ($G(I_{AE})$) with mean μ and standard deviation σ is used to describe the pixel intensities within the AE. The concept of this AE is to iteratively expand or contract on each major axis independently, according to four different forces.

An AE was first introduced for medical ultrasound in [6], where the forces were based on modified Gaussian functions. However, such smooth functions may not be appropriate to distinguish the FLL boundaries precisely. Furthermore, contraction was not allowed, but only expansion, as its force functions were non-negative (Fig. 2(a)). Therefore, we propose alternative force functions for updating the AE on each iteration based on a rectangular function ($Rect_{2\sigma}(I(p_k))$), which is positive for pixel intensities within one standard deviation σ of the mean μ of $G(I_{AE})$, but negative otherwise.

$$Rect_{2\sigma}(I(p_k)) = \begin{cases} +1 & \text{if } \mu-\sigma \leq I(p_k) \leq \mu+\sigma \\ -1 & \text{if } I(p_k) \leq \mu-\sigma \text{ , or } I(p_k) \geq \mu+\sigma \end{cases} \tag{1}$$

where $I(p_k)$ is the intensity of the pixel p_k and 2σ specifies the width of the rectangular function. After considering that the boundary of the AE is divided in K equally-spaced points, then the pixel p_k is in the k^{th} of the K points in this boundary.

The sharpness of $Rect_{2\sigma}(I(p_k))$ is more appropriate for emphasising the FLL's boundaries than the modified Gaussian function proposed in [6], and should allow faster expansion and contraction. The force proposed here is defined as:

$$f_g = \sum_{k=1}^{K} Rect_{2\sigma}(I(p_k)) \cdot W_g\left(\frac{k}{K}\right) \quad , \quad \forall g \in \{x_+, x_-, y_+, y_-\} \tag{2}$$

where x and y are the horizontal and vertical forces with the '$+$' and '$-$' subscripts depicting the direction of each of them, and W_g are the weightings used on each force as defined in [6].

The method is initialised by one seed-point within the FLL region. An elliptical shape model $e(x_c, y_c, r_x, r_y)$ is then employed, where x_c, y_c define the centre of gravity (CoG) and r_x, r_y the semi-major axes of the AE. For updating the CoG and the semi-major axes of the AE, at each iteration i, we propose the following equation.

$$\begin{bmatrix} \Delta x_{c,i} \\ \Delta y_{c,i} \\ \Delta r_{x,i} \\ \Delta r_{y,i} \end{bmatrix} = \begin{bmatrix} \alpha & -\alpha & 0 & 0 \\ 0 & 0 & \alpha & -\alpha \\ \alpha & \alpha & 0 & 0 \\ 0 & 0 & \alpha & \alpha \end{bmatrix} \begin{bmatrix} f_{x+} \\ f_{x-} \\ f_{y+} \\ f_{y-} \end{bmatrix} \tag{3}$$

where each Δ represents the change in the corresponding quantity during that iteration and α is an acceleration parameter. This allows an automated update of the AE, based entirely on the forces obtained directly from the intensity distribution of the image.

Updating the position and shape of the AE terminates if either a maximum number of iterations is reached or if the sum of the magnitudes of the forces and the values of μ and σ all converge, i.e. the changes in them each stay below a specified tolerance over three successive iterations. The final output ellipse (e_{AE}) of the AE process covers the area A_{AE}.

2.2 Boundary Refinements using a Probabilistic Model

This probabilistic boundary refinement (PBR) step is initialised by e_{AE} and considers a non-parametric generic shape model of a closed contour with K points. Initially, another ellipse is created (e_{EXT}), concentric with e_{AE} but with double its semi-major axes and covering an area A_{EXT} (Fig. 2(b)). The annular-shaped area $A_{ring} = A_{AE}^{C} \cap A_{EXT}$ is then defined, and the pixel populations inside each of A_{AE} and A_{ring} are assumed to describe the classes of the FLL and parenchyma, respectively, i.e. C_F or C_P. The segmentation of the FLL's boundary is then treated as a binary classification problem, allocating pixels to either C_F or C_P.

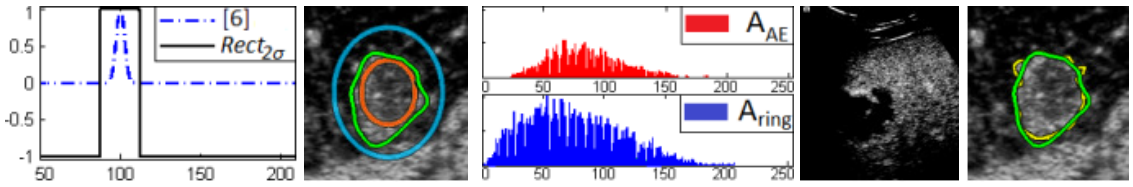

Figure 2: (a) shows the 2 different force functions applied to the AE. In (b) the red (inner) ellipse is e_{AE} and the concentric blue (outer) ellipse is e_{EXT}. The green (irregular-shaped) contour depicts the final segmentation of the FLL by the proposed method (F_d). (c) shows the histogram of the pixel brightness intensities of the two areas of interest (A_{AE} and A_{ring}). (d) shows an FLL not well-distinguished due to acoustic shadow. (e) gives the comparison of F_d (green) compared with the manually annotated ground truth F_{GT} (yellow) giving $J = 84\%$.

Two distinct Gaussian probability distributions are used to model the pixel intensities inside A_{AE} and inside A_{ring}, respectively (Fig. 2(c)). Specifically, the proposed approach processes samples from the population of each class separately, and models the class-conditional probabilities ($Pr(I(p_k)|C_F)$ and $Pr(I(p_k)|C_P)$) by fitting a Gaussian model, using Maximum Likelihood Estimation to find the mean and standard deviation, for each class.

Consequently, at each iteration, the intensity $I(p_k)$ of each boundary point p_k is assessed and $Pr(I(p_k)|C_F)$ compared with $Pr(I(p_k)|C_P)$. This point p_k is classified into C_F or C_P according to the larger of the conditional probabilities. (This is equivalent to a Bayesian classification with equal priors for the two classes.) The contour is then expanded or contracted along the radial line from the CoG to p_k, based on the above classification decision.

The updating of the position and shape of the closed contour terminates if either a maximum number of iterations is reached or if the contour's length converges over five successive iterations, i.e. the changes in the length stay below a specified tolerance.

3 Data and Evaluation Metrics

Data of 60 real clinical cases of a multi-centre study with patients in different physical conditions were provided. 5 cases had to be excluded from the evaluation since the FLL was not well-distinguished from the remainder of the image plane due to acoustic shadows (Fig. 2(d)). All data was acquired using Siemens ACUSON Ultrasound (US) systems (Mountainview CA). 46 cases were captured at King's College Hospital in the UK, at spatial resolution 1024×768 pixels, using an S2000 US system equipped with 4 (or) 6 MHz curvilinear transducer. The remaining 14 cases were captured at Evgenidion Hospital in Greece, at spatial resolution 768×576 pixels, using a Sequoia C512 US system equipped with 6-2 MHz curvilinear transducer. In all examinations the second generation contrast medium SonoVue [8] (Bracco S.p.A., Italy) was used in a 2.4ml bolus intravenous injection (into an arm vein), which allows excellent depiction of the FLL vascularity and perfusion [12]. Specific acquisition parameters of the equipment for each patient are unknown, as they were set by the radiologist individually at the start of each examination. The acquisition method of this data reflects true clinical practice and leads to increased variability. Examinations were performed by radiologists with 13-16 years of experience using CEUS. All data were obtained without prior knowledge of subsequent processing by a software tool and without any specific instructions being given to the radiologist beforehand. Appropriate ethics and confidentiality procedures have been followed at all times.

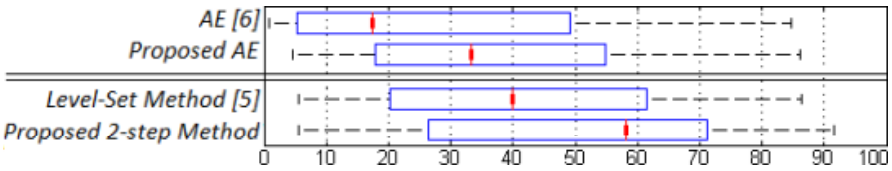

Figure 3: Jaccard index for assessing the overlap between F_{GT} and F_d for the original AE [6], the Level-Set method [5] and the proposed method across our datasets.

To evaluate quantitatively the proposed method at the pixel level, the ground truth silhouettes of the FLLs (F_{GT}) were manually annotated by a radiologist in the reference frame. These silhouettes are then compared with the areas segmented by the proposed method, F_d (Fig. 2(e)). The metric considered for evaluating the similarity and difference between F_{GT} and F_d is the Jaccard index ($J = \frac{|F_{GT} \cap F_d|}{|F_{GT} \cup F_d|}$), as it strictly accepts information only from pixels $p_{x,y} \in F_{GT} \cap F_d$ and penalises pixels misclassified as either FLL or non-FLL ($p_{x,y} \in F_{GT} \triangle F_d$).

4 Experiments and Results

Our proposed methods, along with the original AE [6] and a Level-Set method [5] for comparison, were implemented in Matlab v.7.12 without parallelism on an Intel i7-2620M platform with 8GB RAM and applied to 55 cases where the FLL was well-distinguished. The value of the acceleration parameter α in Eq.3 was set equal to 1 in all cases.

Comparing the median values and inter-quartile ranges (IQR) of J between our enhanced AE and the AE of [6] justifies the proposed improvements (Fig. 3). In addition to the principal improvement, which is the increase in the value of J, the enhanced AE needs on average only 59.4% of the time required for the AE of [6] to converge, namely 1.2 rather than 2 seconds on average per case, as the rectangular force functions lead to faster ellipse fitting. This could be significant where a large number of cases are processed.

Applying the proposed PBR step to the output from the AE (e_{AE}) gives further improvement to J, indicating a much better segmentation of the FLL (Fig. 2(b)). The results from the application of PBR are compared with results of a Level-Set method [5], again initialised by e_{AE}. Both the median and IQR of J across all cases are higher for PBR than for the Level-Set method, showing that the FLL segmentation is superior when using the former. Last but not least, our method converges in a small fraction (2.2%) of the time required by the Level-Set method, e.g. 5.9 seconds rather than 4.4 minutes on average per case.

5 Conclusions and Future Work

In this paper, we proposed a complete pipeline to automate the initialisation tasks required for the evaluation of FLLs in CEUS data. In particular, a novel two-step method was proposed for automating the FLL segmentation based on a probabilistic model. The first step consists of an enhanced AE using a rectangular force function, to approximate the FLL by an ellipse. The second step is used for refining this approximation by iteratively classifying boundary pixels according to a probabilistic model. Experimental comparison of the proposed version of AE to the original one [6] justifies the proposed enhancements. In addition, the second step of our method demonstrated better performance and lower computational time when compared with Level-Sets [5]. However, its performance is dependent on the manual input of one seed-point and the ROI should be in a form which can be reasonably well-bounded by a closed contour. The proposed method should also be appropriate to other modalities and application areas, e.g. breast US. Last but not least, coupling of the proposed pipeline

with an existing tracking method [1, 7, 10] could lead to an automated framework for FLL evaluation providing a second-opinion tool to radiologists.

References

[1] S. Bakas, A. Hoppe, K. Chatzimichail, V. Galariotis, G. Hunter, and D. Makris. Focal Liver Lesion Tracking in CEUS for Characterisation Based on Dynamic Behaviour. *Springer, Advances in Visual Computing*, LNCS(7431):32–41, 2012.

[2] S. Bakas, G. Hunter, C. Thiebaud, and D. Makris. Spot the Best Frame: Towards Intelligent Automated Selection of the Optimal Frame for Initialisation of Focal Liver Lesion Candidates in Contrast-Enhanced Ultrasound Video Sequences. *9th International Conference on Intelligent Environments (IE'13 - Athens, Greece)*, pages 196–203, 2013.

[3] M. Blachier, H. Leleu, M. Peck-Radosavljevic, D.-C. Valla, and F. Roudot-Thoraval. The Burden of Liver Disease in Europe - A Review of Available Epidemiological Data. *European Association for the Study of the Liver*, 2013.

[4] M. Kass, A. Witkin, and D. Terzopoulos. Snakes: Active Contour Models. *International Journal of Computer Vision*, 1(4):321–331, 1988.

[5] C. Li, C. Xu, C. Gui, and M. D. Fox. Distance Regularized Level Set Evolution and Its Application to Image Segmentation. *IEEE Trans Image Proces*, 19(12):3243–54, 2010.

[6] M. Marsousi, J. Alirezaie, A. Ahmadian, and A. Kocharian. Segmenting Echocardiography Images using B-Spline Snake and Active Ellipse Model. *Conf Proc IEEE Eng Med Biol Soc*, 2010:3125–3128, 2010.

[7] N. Rognin, R. Campos, J.-P. Thiran, T. Messager, A. Broillet, and P. Frinking et al. A New Approach For Automatic Motion Compensation For Improved Estimation of Perfusion Quantification Parameters in Ultrasound Imaging. *The 8th French Conference on Acoustics (Tours, France)*, pages 61–65, 2006.

[8] M. Schneider. Charasteristics of SonoVue. *Echocardiography*, 16(7):743–746, 1999.

[9] D. Strobel, K. Seitz, W. Blank, A. Schuler, C. F. Dietrich, and A. vonHerbay et al. Tumor-Specific Vascularization Pattern of Liver Metastasis, Hepatocellular Carcinoma, Hemangioma and Focal Nodular Hyperplasia in the Differential Diagnosis of 1349 Liver Lesions in Contrast-Enhanced Ultrasound. *Ultraschall Med*, 30(4):376–82, 2009.

[10] C. N. Ta, Y. Kono, C. V. Barback, R. F. Mattrey, and A. C. Kummel. Automating Tumor Classification With Pixel-by-Pixel Contrast-Enhanced Ultrasound Perfusion Kinetics. *J Vac Sci Technol B Nanotechnol Microelectron*, 30(2):02C103–01–10, 2012.

[11] M. E. Westwood, M. A. Joore, J. P. C. Grutters, W. K. Redekop, N. Armstrong, and K. Lee et al. Contrast-Enhanced Ultrasound Using SonoVue®(Sulphur Hexafluoride Microbubbles) Compared With Contrast-Enhanced Computed Tomography and Contrast-Enhanced Magnetic Resonance Imaging for the Characterisation of Focal Liver Lesions and Detection of Liver Metastases: a Systematic Review and Cost-Effectiveness Analysis. *Health Technol Assess*, 17(16), 2013.

[12] S. R. Wilson and P. N. Burns. Microbubble-Enhanced US in Body Imaging: What Role? *Radiology*, 257(1):24–39, 2010.